MRS Advances © 2018 Materials Research Society
DOI: 10.1557/adv.2018.43

Multiple Metamaterial Pattern Integration for Polarization Selective Photodetector Applications

Corey Shemelya[1,2], Nicole A. Pfiester[1], Dante DeMeo[1], Thomas Rotter[3], Ganesh Balakrishnan[3], and Thomas E. Vandervelde[1]*

[1] *Electrical and Computer Engineering Department, Tufts University, 161 College Ave. Medford MA, 02155, U.S.A.*

[2] *Electrical and Computer Engineering Department, The Technical University of Kaiserslautern, Erwin-Schrödinger-Straße 1, 67663 Kaiserslautern, Germany*

[3] *Electrical and Computer Engineering Department, The University of New Mexico, 1313 Goddard SE, Albuquerque, NM 87106, U.S.A.*

*tvanderv@ece.tufts.edu

ABSTRACT

Interest in active metamaterial (MM) devices has recently increased due to their potential for tunable, switchable, and scalable optical responses. More specifically, a dynamic, on-chip MM polarizer has applications ranging from material characterization to sensing without the need for cumbersome external filters. This work demonstrates efforts to optimize MM devices for dynamic polarization filtering by combining elements from split-ring resonators, wire-pairs, and fishnet patterns. The polarization grid has been designed to operate under an applied voltage with simulated on/off ratios of 75% and dynamic polarization selectivity of 70%. Samples have been fabricated using epitaxial GaAs on sapphire with various n-type doping concentrations to approximate electrical tuning.

INTRODUCTION

The first metamaterials, the split ring resonator (SRR), operated exclusively at GHz frequencies; however, recent research utilizing various micro/nano-fabrication methods have resulted in metamaterials (MMs) designed to operate at visible and infrared (IR) frequencies [1-3]. Although there are many MM designs, of particular interest to this work are the SRR, optical fishnet, and wire-pair metamaterial designs [1,2,4]. These structures maintain many similarities and difference. For example, incremental modification of the SRR led to comparison with repeating patterns of nano-bars [4,5]. Nano-bars have since become known as split-wire pairs (SWPs). Like SRRs, SWPs operate as notch filters with a high transmission window and large absorption at

resonance [5]. Therefore, the SWPs generally provide polarization sensitivity similar to metallic gratings typically used in polarization grids [6,7]. Optical fishnets, by comparison, generate a bandpass resonant response, and utilize two metallic layers with a dielectric spacer. The thickness of these layers plays a large role in the final response, and as such require careful design. Repeating patterns of circular or square holes are then etched through the structure, creating an MM which excels at narrow band transmission [8,9].

This work aims to combine these three designs to produce a polarization-dependent MM response which can lead to photodetector diode-compatible technologies [10, 11], enabling the creation of a fully chip integrated polarimeter [12]. Specifically, this work aims to create an MM polarization grid capable of dynamic on/off states, with the potential monolithic integration of multiple grids for full polarization selectivity. In order to show the potential for an altered optical response with an applied external voltage, a thin-film semiconductor is used as the active layer in the unique MM structure. This structure can then utilize the properties of multiple metamaterials to selectively filter a single polarization, allowing the orthogonal polarization to pass unhindered, resulting in potential design for a MM frequency selective dynamic polarizer.

EXPERIMENTAL DETAILS

The optical response of a metamaterial is dependent on its effective permittivity, and effective permeability [13, 14], which is determined by several design elements. For example, the effective permeability, μ_{eff}, and permittivity, ε_{eff}, of a circular MM SRR can be given by Equations 1 and 2 [13,14],

$$\mu_{eff} = 1 - \frac{\pi r^2}{a^2 \left(1+\frac{2\sigma}{wr\mu_0}i-\frac{3}{\pi^2\mu_0 w^2 Cr^3}\right)} \quad (1)$$

$$\varepsilon_{eff} = 1 - \frac{w_p^2}{w^2} \quad (2)$$

where σ is conductivity, w is wave frequency, r is ring radius, a is the MM lattice constant, w_p is the plasma frequency of the metal, and C is the capacitance of the split-gap. This capacitance is directly related to the conductivity of the split gap (σ_g). By modelling the capacitance of the SRR as a parallel-plate capacitor, we see that a large change in the ratio between voltage and current will result in a change in gap conductivity, as shown in Equation 3,

$$\sigma = {}^{J}/_{\boldsymbol{E}} = \frac{I/A}{V/l} = \frac{Il}{VA} \quad (3)$$

where J is the current density, E is the electric field, A is the cross-sectional area, and l is the length. Previous work in the field has utilized a reverse bias Schottky diode to alter the current to voltage ratio, increasing V much more than I [15-20]. However, inspection of Equation 3 allows for one to also increase I more than V by applying a forward bias to the same Schottky diode system and achieve a similar change in gap conductivity. This work looks to apply the latter method of dynamic switching to create the proposed MM polarizer.

To achieve polarization selectivity there must be: (1) an independent transmission characteristic for each incident polarization and (2) an independent resonance near the same frequency for both orthogonal polarizations. These conditions allow the device to operate at a single frequency, and when optimized, display near perfect transmission or

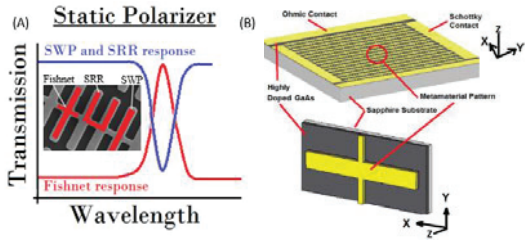

Figure 1. (A) Desired orthogonal optical response of the three incorporated MM designs (inset). (B) Dynamic device schematic with substrate, GaAs layer, and MM pattern between two contacts.

absorption, Figure 1a. To satisfy these constraints, elements from three MM structures were combined; SRRs, SWPs, and optical fishnets, shown in the insert of Figure 1a.

Combining the parallel metallic bands of an SWP, the ring resonator design of SRR, and the repeating "+" of a fishnet pattern resulted in the MM pattern shown in Figure 1. A Schottky barrier formed between the metallic pattern and the semiconductor layer was used to imitate an optical fishnet, with an electrical Schottky barrier replacing the dielectric barrier. The expected result was an MM resonance from the anisotropic SRR, high transmission and polarization sensitivity from the SWP, and low transmission polarization sensitivity from the fishnet pattern. These properties allowed for a high transmission resonance with one polarization and a high absorption resonance for an orthogonal polarization. Figure 1a describes the position of each MM structure in the polarizer as well as the expected response for the resulting structure. Additionally, this work separates the results into X and Y polarizations as defined on the axis shown in Figure 1(b).

The fabricated device uses a sapphire substrate to maximize signal transmittance, though it was not included in the simulations as it does not impact the specific MM responses. However, one should note that the sapphire will reduce final transmission by 20% over all operating wavelengths. On top of the sapphire, a layer of epitaxial GaAs semiconductor layer was simulated as the source of the dynamic response. CST Microwave Studio was used to simulate and optimize the structure stack prior to device fabrication, Figure 1b. In the fabricated structure, the thin film GaAs layers were grown via molecular beam epitaxy; electron beam lithography was used for the MM pattern; and photolithography was used for the contact pads. All metallizations were performed with electron beam evaporation.

RESULTS

Semiconductor thickness played a large role in creating the MM polarizer, as seen when calculating the real and imaginary index of refraction (Equations 4 and 5).

$$Im(n) = \pm Im\left(\frac{\cos^{-1}\left(\frac{1}{2t}[1-r^2-t^2]\right)}{kd}\right) \quad (4)$$

$$Re(n) = \pm Re\left(\frac{\cos^{-1}\left(\frac{1}{2t}[1-r^2-t^2]\right)}{kd}\right) + \frac{2m\pi}{kd} \quad (5)$$

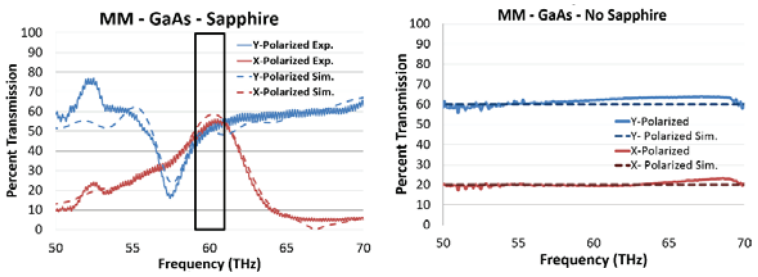

Figure 2. (A) Experimental and simulated MM transmission response for X and Y polarized light. The frequency region of interest is highlighted. (B) Fabrication on bulk n-type GaAs eliminates the MM response.

In these equations, d is the thickness of the MM, k is the incident wavevector, t is the normalized transmission coefficient, r is the normalized reflection coefficient, and m is an integer used to correct branch errors [21]. From these equations, one can see that under certain i.e. when semiconductor thickness is too large, the effective parameters approach that of a bulk semiconductor, and not the designed metasurface. However, in practice, the semiconductor must also be thick enough to allow sufficient induced surface current and conductivity for electron beam lithography and stable electrical contacts. A compromise of a 400 nm thick layer of GaAs was used, with a Ti/Au (8nm/92nm) MM structure.

To determine polarization sensitivity, the structure was exposed to X-polarized (parallel to MM bar) and Y-polarized (perpendicular to MM bar) light in an FTIR. As shown in Figure 2a, the resulting structure acts as a static band pass for both polarizations at 60 THz, the operational frequency range for many IR photodetectors. To verify that the response is due to the combination GaAs/sapphire substrate, this MM was also constructed on a 450 μm thick bulk GaAs substrate. In the control substrate there is a loss of carrier confinement near the surface of the GaAs and an uncoupling of the thin film MM effect, shown in Figure 2b. The resulting response is similar to that of a traditional metallic polarization grid.

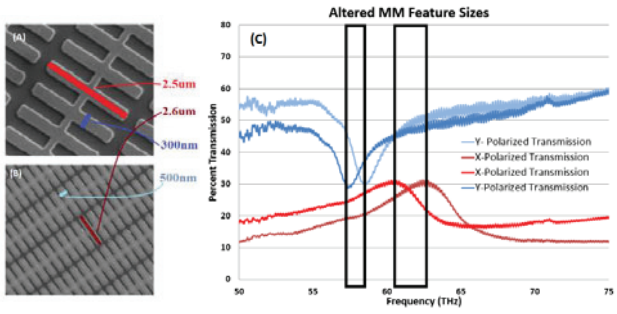

Figure 3. Altering the X and Y dimensions of the MM (A),(B) changes the transmission characteristics for the corresponding orthogonal polarizations (C).

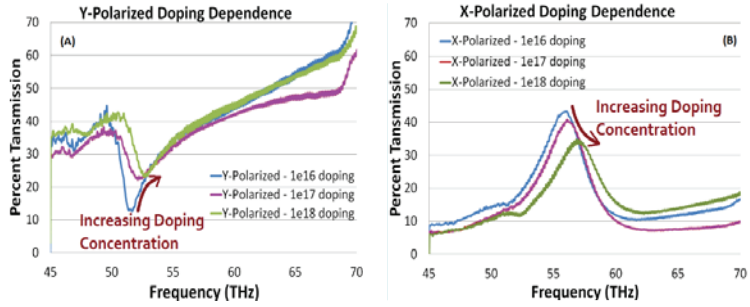

Figure 4. An increase in carrier concentration will shift resonance and increase/decrease transmission for both Y- (A) and X-polarized (B) light.

Additionally, altering the MM gap spacing in the X and Y direction uniquely affects the MM response, as seen in Figure 3. Therefore, each polarization's resonance frequency can be adjusted independently by altering these dimensions. When optimized, this orthogonality can allow for designer regions of unity transmission, effectively allowing one to increase or decrease the operational frequencies of the filter on demand.

As this structure was designed with the potential ability to operate with an applied bias, initial work was undertaken to show the effect of increased carrier concentration. By increasing substrate doping levels, one can approximate the carrier injection observed through a forward biased Schottky diode. The previously described MM pattern was fabricated on three GaAs substrates with n-type doping ranging from $1x10^{16}$ to $1x10^{18}$ /cm^3. Experimental results show a lower change in conductivity than expected through simulation. However, some noticeable changes are observed, such as a shift in resonance frequency and a decrease in resonance strength for each polarization, shown in Figure 4.

CONCLUSIONS

By implementing a unique combination of traditional MM designs, this work outlined and tested a unique structure that demonstrated a high transmission notch filter for Y-polarized light and a low transmission bandpass filter for X-polarized light. The sapphire/GaAs/metallization stack was confirmed to produce the desired static MM effect through experimental testing on bulk GaAs, and the static MM structure was shown to produce 1:1 transmission for both polarizations at a frequency of 61 THz (4.9 μm). The potential for conversion to a dynamic MM polarization grid was demonstrated by increasing GaAs dopant concentration to simulate a forward biased Schottky diode. The result was a decrease in transmission for the "filtered" polarization and a constant transmission for the "pass band" polarization. By continuing this work towards electrically switchable devices, new breakthroughs can lead to photodetectors with on-chip dynamic polarizing grids, eliminating the need for fixed polarization grids on a pixel or bulky external polarization filter wheels.

ACKNOWLEDGMENTS

We would like to thank the National Science Foundation (NSF) (#ECCS-1055203), the Air Force Office of Scientific Research (#FA9550-11-10061), the Office of Naval Research (#N00014-15-1-2946), and The Alexander von Humboldt Foundation. This work was performed in part at the Center for Nanoscale Systems at Harvard University, a member of the National Nanotechnology Coordinated Infrastructure Network (NNCI), which is supported by NSF #1541959. This work was also performed in part at the Tufts University Micro-/Nano-Fabrication Facility and the Center for High Technology Materials at The University of New Mexico. This research was supported in part by an appointment to the Intelligence Community Postdoctoral Research Fellowship Program at Tufts University administered by Oak Ridge Institute for Science and Education through an interagency agreement between the U.S. Department of Energy and the Office of the Director of National Intelligence. It was also supported by the NSF Graduate Research Fellowship Program under Grant No. GRFP1000169618. Any opinions, findings, and conclusions or recommendations expressed are those of the author(s) and do not necessarily reflect the views of the NSF.

REFERENCES

1. M. Husnik, S. Linden, R. Diehl, J. Niegemann, K. Busch, and M. Wegener. *Phys. Rev. Lett.* **109**, 233902 (2012).
2. F. von Cube, S. Irsen, R. Diehlet, J. Niegemann, K. Busch, and S. Linden. Nano Lett. **13**, 2 (2013).
3. B. Kanté, S. N. Burokur, F. Gadot, and A. de Lustrac. Proc. of SPIE Vol. 6987, 69870F-1 (2008).
4. A. Rottler, M. Harland, M. Broll, S. Schwaiger, D. Stickler, A. Stemmann, C. Heyn, D. Heitmann, and S. Mendach. Appl. Phys. Lett. **100**, 151104 (2012).
5. X. Wei, H. Shi, X. Dong, Y. Lu, and C. Du. Appl. Phys. Lett. **97**, 011904 (2010).
6. X. Hu, M. Li, Z. Ye, W. Y. Leung, K.-M. Ho, and S.-Y. Lin. Appl. Phys. Lett. **93**, 241108 (2008).
7. M. Guillaumée, L. A. Dunbar, C. Santschi, E. Grenet, R. Eckert, O. J. F. Martin, and R. P. Stanley. Appl. Phys. Lett. **94**, 193503 (2009).
8. N. Dutta , I. O. Mirza, S. Shi, and D. W. Prather. Materials **3**, 5283-5292 (2010).
9. M. R. Shcherbakov, P. P. Vabishchevich, T. V. Dolgova. A. A. Zaitsev, A. S. Sigov, and A. A. Fedyanin. Proc. of SPIE, Vol. **7353** (2009).
10. C. Downs and T.E. Vandervelde, Sensors, **13**, 4, 5054-5098 (2013).
11. J. Rosenberg, R. V. Shenoi, T. E. Vandervelde, S. Krishna, and O. Painter, App. Phys. Lett. **95**, 161101 (2009)
12. N. Pfiester, C. Shemelya, T. Rotter, G. Balakrishnan, T. E. Vandervelde, Proc. SPIE 8982, Optical Components and Materials XI, 89820M (2014).
13. J. B. Pendry, A. J. Holden, D. J. Robbins, and W. J. Stewart. IEEE Trans. on Microwave Theory and Techniques **47**, 11 (1999).
14. J. B. Pendry, A. J. Holden, D. J. Robbins, and W. J. Stewart. J. Phy. Condens. Matt. **10**, 4785-4809 (1998).
15. O. Hess, J. B. Pendry, S. A. Maier, R. F. Oulton, J. M. Hamm, and K. L. Tsakmakidis. Nature Mat.**11**, 573-584 (2012).
16. J. Gu, R. Singh, A. K. Azad, J. Han, A. J. Taylor, J. F. O'Hara, and W. Zhang. Opt. Mat. Exp., Vol. 2, No. 1, January (2012).
17. W. J. Padilla, A. J. Taylor, C. Highstrete, Mark Lee, and R. D. Averitt. Phys. Rev. Lett., **96**, 107401 (2006).
18. E. Kim, W. Wu, E. Ponizovskaya, Z. Yu, A. M. Bratkovsky, S.-Y. Wang, R. S. Williams, and Y. R. Shen. Appl. Phys. Letts. **91**, 173105 (2007).
19. H.-T. Chen, W. J. Padilla, M. J. Cich, A. K. Azad, R. D. Averitt, and A. J. Taylor. Nature Photonics, **3**, 148-151 (2009).
20. H.-T. Chen, J. F. O'Hara, A. K. Azad, A. J. Taylor, R. D. Averitt, D. B. Shrekenhamer, and W. J. Padilla. Nature Photonics, **2**, 295-298 (2008).
21. D. R. Smith, S. Schultz, P. Markos, C. M. Soukoulis. Phys. Rev. B **65**, 195104 (2002).